Journal of Materials Chemistry A

ROYAL SOCIETY OF CHEMISTRY

COMMUNICATION

View Article Online
View Journal | View Issue

Cite this: J. Mater. Chem. A, 2023, 11, 18660

Received 14th July 2023
Accepted 17th August 2023

DOI: 10.1039/d3ta04161a

rsc.li/materials-a

Supramolecular reinforcement drastically enhances thermal conductivity of interpenetrated covalent organic frameworks†

Sandip Thakur and Ashutosh Giri *

Covalent organic frameworks (COFs) are an emerging class of polymeric crystals with immense permanent porosities and large surface areas that are highly sought after for a variety of applications such as in heterogeneous catalysis, flexible electronics, and gas separation and storage. Although efficient heat dissipation plays a critical role in such applications, thermal transport in COFs has frequently been overlooked or has been an afterthought. Herein, we investigate the heat transfer mechanisms in the prototypical 3D COF-300 and demonstrate that interpenetration of the organic frameworks can result in dramatic enhancements in the heat transfer efficacies facilitated through supramolecular interactions between the individual frameworks. More specifically, we show that a 3-fold interpenetration can lead to as much as 6-fold increase in the room temperature thermal conductivity of COF-300. We attribute this to phonon hardening and reduced vibrational scattering at the pores resulting from the reinforcement due to supramolecular interactions that rigidify the individual frameworks in the interpenetrated structures. We also show that these materials possess ultralow and modular elastic moduli, thus positioning them as materials that are both lightweight and mechanically flexible, all the while maintaining relatively high thermal conductivities.

Combining multifunctional properties such as high thermal conductivity, mechanical flexibility, electrical insulation, and ultralight-weight characteristics in one material system has the potential to revolutionize the further advancements in the next-generation of technologies such as integrated circuits,[1,2] wearable electronics,[3,4] soft machines,[5] flexible solar cells,[6,7] sensors,[8] and biomedical applications.[9] However, incorporating these physical attributes in one material system has proven to be a difficult task and currently is one of the most sought-after fundamental scientific challenges. For instance, thermally conductive materials are conventionally rigid and dense (with a high elastic modulus as shown in Fig. 1), which makes them impractical for several of the aforementioned applications where flexibility and low densities are critical prerequisite properties. In this regard, porous coordination polymers such as metal–organic frameworks (MOFs) and covalent-organic frameworks (COFs) have shown great promise as multifunctional, designer materials that can combine several unrivaled physical properties in one material system.[1,10–17] For example, Evans *et al.*[1] have recently demonstrated

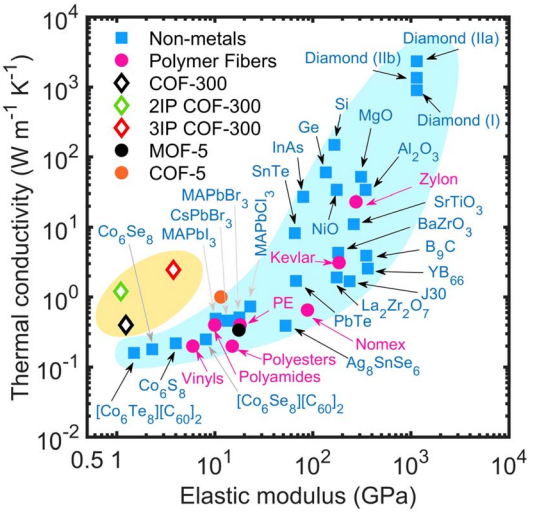

Fig. 1 Comparison of thermal conductivity as a function of elastic modulus for a wide range of materials at room temperature. Conventionally, materials with higher elastic modulus are associated with higher thermal conductivities because these materials have more rigid and dense crystal structures that are held together by stronger bonds. COFs are an emerging class of materials that possess low densities (with reduced elastic moduli) along with relatively higher thermal conductivities. Interpenetration of COFs can lead to dramatic enhancement in their thermal conductivities all the while maintaining their mechanical flexibility (as shown by the 6-fold enhancement in thermal conductivity for a 3-fold interpenetrated COF-300 structure).

Department of Mechanical, Industrial and Systems Engineering, University of Rhode Island, Kingston, RI 02881, USA. E-mail: ashgiri@uri.edu

† Electronic supplementary information (ESI) available: Details on Equilibrium MD (EMD) simulations, Non-equilibrium MD (NEMD) simulations, vibrational density of states, elastic moduli (E) and thermal conductivities (κ) of different materials at room temperature. See DOI: https://doi.org/10.1039/d3ta04161a

that boronate ester-linked 2D COF thin films are endowed with low dielectric constants and possess a room temperature thermal conductivity of ~1 W m^{-1} K^{-1} (Fig. 1) along the laminar pores, marking a new paradigm in materials design that combines relatively high thermal conductivity with low mass density. Herein, we add to the remarkable attributes of COFs by demonstrating that interpenetration of 3D COFs results in dramatic enhancements in their thermal conductivity through supramolecular interactions all the while preserving their low elastic modulus. This positions interpenetrated COFs as light-weight materials that are mechanically flexible yet thermally conductive, a combination of physical properties which are typically not found in most material systems as highlighted in Fig. 1.

Although interpenetrated or entangled networks of 3D COFs have been synthesized in the past,[18–23] the impact of intertwining several COF lattices on the resulting physical properties such as their mechanical and thermal properties has not yet been investigated. This is in contrast to their MOF-cousins where the impact of interpenetration has not only been shown to lead to the formation of intricate architectures,[24–27] but has also been related to enhanced stabilities, added structural flexibilities and higher gas adsorptions as compared to a single MOF lattice.[28,29] Furthermore, interpenetration of idealized MOFs has also been shown to increase their thermal conductivity through additional channels of heat transfer.[30,31]

In terms of why the understanding of thermal transport processes in porous polymeric frameworks are of interest: since these materials are widely used for gas storage and chemical separations, enhancement in their thermal transport is mainly sought after to mitigate the excess heat generation that occurs during adsorption of guest species inside the open frameworks.[32,33] These processes are typically exothermic in nature resulting in temperature excursions of several hundred Kelvins during gas intake and desorption. Moreover, as mentioned above, increasing heat conduction in porous crystals could also lead to their usage in applications involving efficient thermal management strategies for flexible and wearable electronics.[14] In this regard, studies have mainly focused on understanding thermal transport in zeolites and MOFs where the thermal conductivities are mostly reported to be low and glass-like (with values in the range of ~0.3 to 1 W m^{-1} K^{-1}).[32–48] The main reason for the reduced thermal conductivity has been attributed to their low densities and highly porous structures that inhibit thermal transport by reducing the mean free paths of vibrational energy carriers through enhanced scattering at the pores.

With regard to the thermal transport properties of COFs, only a handful of studies (mostly focusing on 2D COFs) have reported on their thermal conductivities.[1,13,14,49,50] These studies have shown that thermal conductivities in COFs are typically higher than in MOFs mainly due to the prevalence of strong covalent bonds that hold light atoms (*e.g.*, C, N, O, and B) in an extended crystalline framework in COFs. In contrast, large atomic mass mismatches in MOFs can lead to considerable impediment to heat conduction through additional vibrational scattering.[34] Although these prior studies have provided significant insight into the thermal transport processes in porous organic frameworks (in general), a comprehensive understanding of the vibrational heat conduction in 3D COFs and the effect of framework interpenetration on their thermal conductivity is still missing. Therefore, understanding the fundamental nature of heat transfer in 3D COFs with an atomic-level perspective on their structure–property relationship along with strategies to improve their overall heat conduction can not only be transformative for the above-mentioned applications, but can also advance our fundamental understanding of thermal transport in porous crystals.

Here, we use reactive molecular dynamics (MD) simulations to study heat transfer mechanisms in the prototypical COF-300 and its interpenetrated structures. We show that the thermal conductivity of COF-300 is anisotropic and highly depends on the orientation of the polymeric chains with respect to the direction of the heat flow. Interpenetration of these polymeric frameworks is shown to drastically enhance their thermal conductivities by as much as 6-fold at room temperature and also leads to the dramatic reduction in anisotropy with a thermal conductivity of ~2.5 W m^{-1} K^{-1} in all directions. We attribute this enhancement to supramolecular interactions between the individual COF-300 frameworks that results in considerable phonon hardening and lattice stiffening. Furthermore, along with the reduction in the anisotropy in thermal conductivity, we show that the thermal conductivity trend with temperature for a 3-fold interpenetrated COF-300 structure demonstrates a more crystalline-like behavior as compared to the single framework. Uniaxial tensile strain simulations show that these materials are mechanically flexible and possess modular elastic moduli (in the range of 1–13 GPa) achieved through interpenetration. Moreover, enhancements in thermal conductivity of the 3-fold interpenetrated structure can be achieved *via* hydrostatic compressions, which reinforces the supramolecular interactions between the individual frameworks and thus provides an efficient strategy to further engineer their modular thermal conductivities. Taken together, our results highlight the key role of interpenetration in COFs that can dramatically modify their physical properties and as shown in Fig. 1, thus positioning them as materials that are both lightweight and mechanically flexible, all the while maintaining high thermal conductivity, which can be highly beneficial for a range of applications such as in the next-generation of flexible electronics.

We begin by first investigating the heat transfer mechanisms in a single COF-300 framework. The schematics of the computational domain for our COF-300 structure along different directions are shown in Fig. 2a. Note, we prescribe the *x*- and *y*-directions as the in-plane direction (since the polymeric chain alignments are identical in the two principal directions) and the *z*-direction as the cross-plane direction for the discussions below. To describe the interatomic interactions, we utilize the reactive potential, ReaxFF,[51] and conduct our MD simulations with the large-scale atomic molecular massively parallel simulator (LAMMPS) package.[52] The choice of the reactive potential allows us to study the effect of supramolecular (or non-bonded) interactions that include van der Waals forces, hydrogen bonding, electrostatic interactions and most importantly, the host–guest interactions that can vary based on the relative

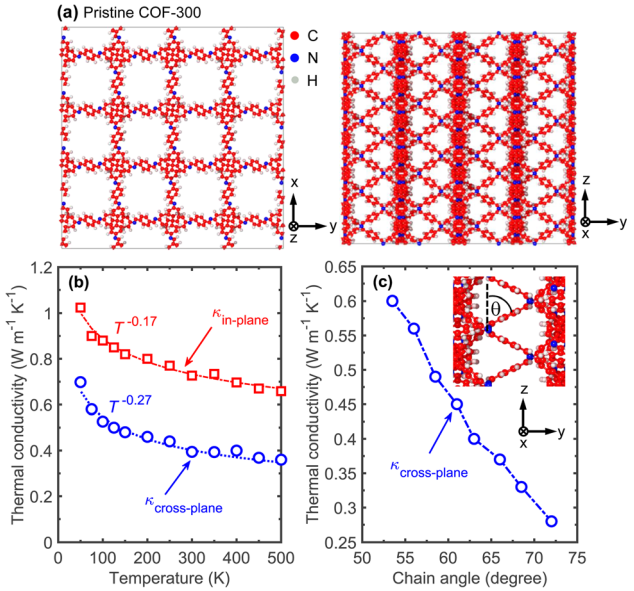

Fig. 2 (a) Schematics of our COF-300 computational domain highlighting the anisotropy along the in-plane (*x*- and *y*-) and cross-plane (*z*-) directions. The chains are better oriented along the two principal in-plane directions, whereas the linkers are at ~60° along the cross-plane direction. (b) Green–Kubo-predicted thermal conductivities as a function of temperature for our pristine COF-300 structure in the in-plane and cross-plane directions. Throughout the temperature range, the in-plane thermal conductivity is twice as high as compared to the cross-plane direction. (c) Thermal conductivities in the cross-plane (*z*-) direction as a function of angle between the polymeric linkers and the cross-plane axis for our pristine COF-300 structure at room temperature. With the decrease in the angle, the polymeric chains are better aligned along the cross-plane direction and thus increasing the heat conduction along that direction.

displacements of the individual COF-300 frameworks with respect to each other in the interpenetrated frameworks. To calculate the thermal conductivities, we utilize the Green–Kubo (GK) formalism under the equilibrium MD simulations framework (see ESI† for further details).

Fig. 2b shows our GK-predicted thermal conductivity as a function of temperature for the COF-300 structure along the in-plane and cross-plane directions. For the entire temperature range, COF-300 possesses an anisotropic thermal conductivity with higher values in the in-plane direction. This can be attributed to better chain alignment in the in-plane direction as compared to the cross-plane where the linkers are oriented ~60° to the *z*-axis (Fig. 2a, right panel). As shown in Fig. 2c, varying the angle of the linker with respect to the cross-plane direction can significantly affect the thermal conductivity in that direction; a better alignment of the linkers along the *z*-axis (where the angle of the linkers are varied systematically as represented in the inset of Fig. 2c) leads to a higher thermal conductivity along that direction. We attribute this enhancement to the better channeling of heat flow through the linkers along the cross-plane direction. Although a modest (~2×) increase in the thermal conductivity of COF-300 can be achieved *via* polymeric chain orientation, a much larger (~6×) enhancement can be attained *via* supramolecular interactions resulting from interpenetration as we detail in the following discussions.

We generate our 2-fold interpenetrated structure by creating a copy of the pristine COF-300 structure and translating it by 5 Å along the three principal directions. Similarly, the 3-fold interpenetrated COF-300 structure is generated by creating two copies of the pristine COF-300 structure and translating the first and second copies by 8 Å and 5 Å, respectively. Fig. 3a and b show the schematics of the interpenetrated structures in the in-plane and cross-plane directions, respectively. The corresponding temperature dependent thermal conductivities as compared to the pristine COF-300 is shown in Fig. 3c and d for the in-plane and cross-plane directions, respectively. Along with the enhancement in thermal conductivity for the entire temperature range, it is interesting to note that interpenetration also leads to a larger dependence on temperature as shown by the increase in the exponent α, where $\kappa \propto T^{-\alpha}$. This suggests that interpenetration reduces the effect of vibrational scattering at the pores (which reduces the temperature dependence)[13,50] and leads to a more crystalline-like temperature dependence; for a pure, defect-free crystalline solid, anharmonic three-phonon scattering leads to a $\kappa \propto T^{-1}$ temperature trend.[53,54] In this regard, the increase in temperature dependence when comparing the results for the 2-fold interpenetrated structure to the 3-fold structure suggests that enhanced supramolecular interactions in the 3-fold case results in the more crystalline-like behavior. Furthermore, as shown in Fig. 3e, the enhanced supramolecular interactions also result in the drastic reduction in anisotropy along the in-plane and cross-plane directions for the entire temperature range. This is because, for the interpenetrated structures, additional channels of heat flow along the cross-plane direction (as shown by the arrows in Fig. 3b) can enhance heat conduction dramatically and compensate for the insufficiencies and the vibrational scattering associated with the linkers that are oriented at 60° with respect to the *z*-axis, which for the case of the single framework, reduces their efficacy to conduct heat along the cross-plane direction.

Next, to gain more insights into the increased heat conduction in our interpenetrated COF-300 structures, we compare the vibrational density of states (DOS) of the pristine and interpenetrated COF-300 structures as shown in Fig. 4a. We observe considerable vibrational hardening throughout the frequency spectrum with interpenetration in our DOS calculations. This shift to higher frequencies, resulting from the interframework interactions, promotes additional heat transfer channels through these higher frequency modes, which could be one of the main reasons for the enhancement in thermal conductivity. The other plausible reason for the enhancement in thermal conductivity might also originate from reduced phonon–phonon scattering processes since the individual frameworks could be "locked in" their equilibrium positions due to the reinforcement from the supramolecular interactions leading to reductions in anharmonic vibrational scattering mechanisms. This is quantitatively shown in Fig. 4b where we compare our calculated mean square displacements (MSDs) of the atoms in our pristine COF-300 and the interpenetrated structures. Throughout the temperature range, interpenetration results in

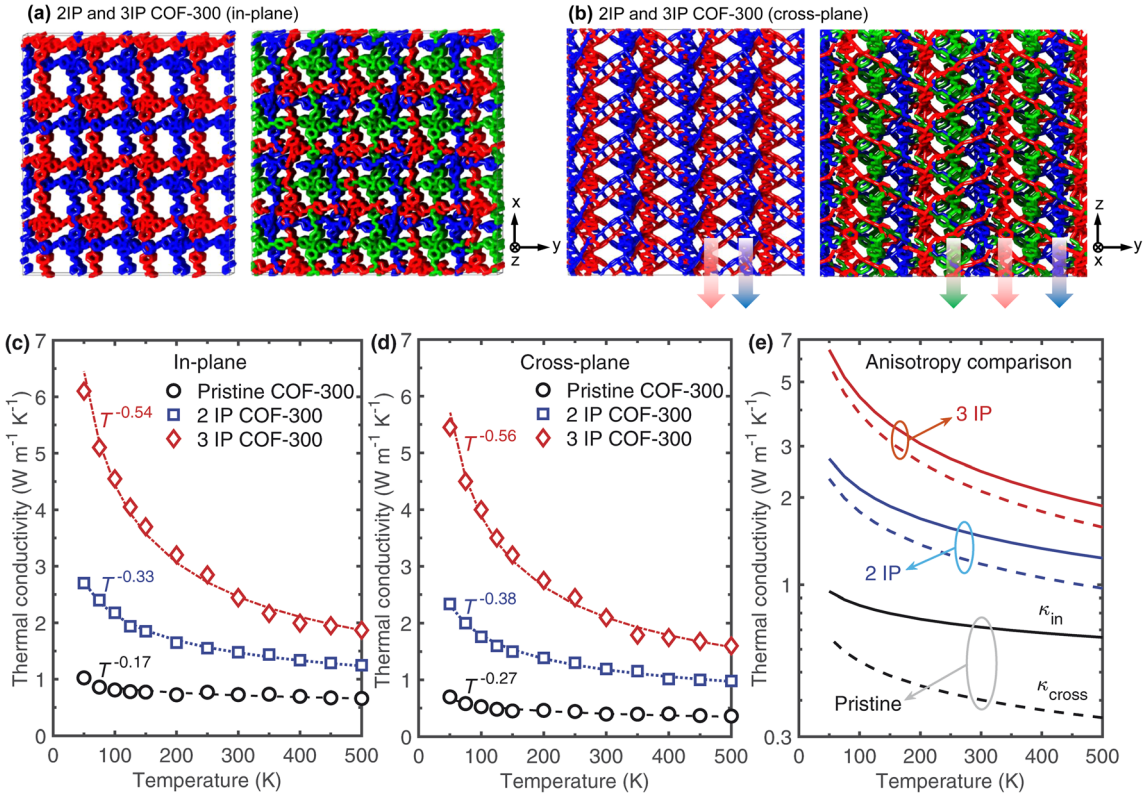

Fig. 3 Schematic illustrations of the computational domains for our (a) 2-fold interpenetration (2IP) and (b) 3-fold interpenetration (3IP) of COF-300 frameworks. Interpenetration of COF-300 frameworks leads to additional channels of heat transfer, which are more prominent in the cross-plane direction as represented by the arrows. Calculated thermal conductivities as a function of temperature for our pristine, 2IP, and 3IP COF-300 structures in the (c) in-plane and (d) cross-plane directions. Along with drastic enhancements in thermal conductivity across the temperature range studied, interpenetration also leads to a larger dependence of thermal conductivity with temperature. This is indicative of a transition to a more crystalline-like behavior with interpenetration where the $\kappa \propto T^{-1}$ trend has been ascribed to anharmonic three-phonon scattering effects in pure crystalline solids. (e) Comparison of anisotropic thermal conductivities as a function of temperature for pristine, 2IP, and 3IP COF-300 structures. Note, the solid and dashed lines represent the in-plane and cross-plane thermal conductivities, respectively. The anisotropy in the thermal conductivity decreases significantly with increasing interpenetration of our COF-300 structures. This can be attributed to the enhanced contribution along the cross-plane direction from the additional channels of heat transfer (represented by the arrows in (b)) that compensates for the vibrational scattering at the misaligned linkers (with respect to the cross-plane direction; inset of Fig. 2c).

reduced MSDs and thus decreased anharmonic effects; since atoms vibrate around their equilibrium positions in solids through thermal fluctuations (k_BT), the more the atom deviates from its equilibrium position, vibrational scattering is further enhanced and the system becomes more anharmonic.[55]

The reinforcing effects of the supramolecular interactions leading to the rigidification of the structures is quantified by the drastic increase in the Young's modulus for the 3-fold interpenetrated COF-300 as shown in Fig. 4c. The elastic modulus of the COF structures are determined *via* additional uniaxial tensile simulations (see Fig. S6†). Note, the in-plane elastic modulus for the COFs are higher than that in the cross-plane since the polymeric chains (with the strong covalent bonds) are oriented better along the in-plane direction (see Fig. 2a, 3a and b). In this regard, although interpenetration reduces the anisotropy in thermal conductivity, the anisotropy in the mechanical properties are still preserved even with a 3-fold interpenetration. Moreover, although interpenetration leads to enhancements in the elastic moduli in both the in-plane and cross-plane directions, the interpenetrated structures are still considerably more flexible as compared to fully dense inorganic solids and are on par with other polymeric materials (albeit with higher thermal conductivities resulting from the extended crystalline frameworks) as highlighted in Fig. 1. Along with the increase in their Young's moduli, the crystallinity is also enhanced from the supramolecular reinforcement in the interpenetrated frameworks. This is quantified by our calculations of the X-ray diffraction patterns at 300 K for pristine and interpenetrated COF-300 structures as shown in Fig. 4d. With the increase in interpenetration, the high intensity peaks also increase confirming their increased crystallinity and the concomitant increase in the temperature dependence of the thermal conductivities (see Fig. 3c and d).

The influence of supramolecular interactions on the thermal transport in interpenetrated COF-300 structures can be appreciated by comparing their thermal conductivities to that of a system of frameworks placed in parallel with an aggregate thermal conductivity that is the sum of their individual frameworks ($3 \times \kappa_{COF\text{-}300}$ that does not include any effects from framework–framework interactions as shown in Fig. 4e and f).

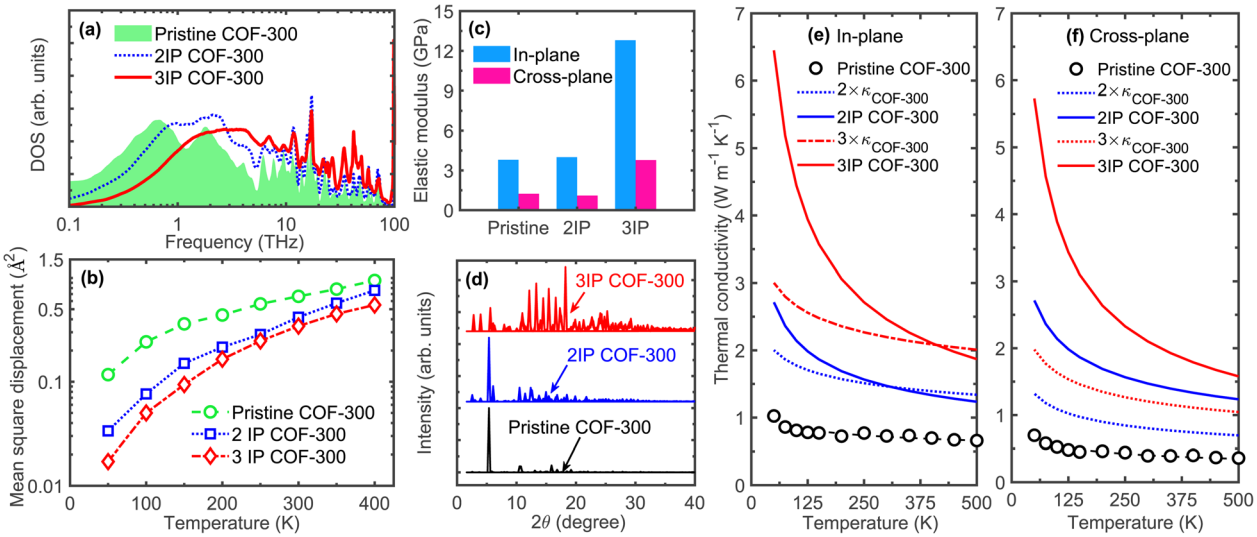

Fig. 4 (a) Vibrational density of states of our pristine, 2IP, and 3IP COF-300 structures. We observe considerable shift in the vibrational spectrum to higher frequencies with the interpenetration of our COF-300 frameworks resulting in phonon hardening of the frameworks. (b) Calculated mean square displacements (MSDs) as a function of temperature for the three computational domains. The MSDs of interpenetrated structures are reduced significantly across the entire temperature range as compared to the pristine COF-300 structure. This supports the considerable hardening of the vibrations, thus resulting in the higher thermal conductivities for the interpenetrated structures as compared to the pristine COF-300 throughout the temperature range (as shown in Fig. 3c and d). (c) Comparison of elastic moduli of our pristine, 2IP, and 3IP COF-300 structures showing a drastic increase with the 3-fold interpenetration. The in-plane Young's modulus is higher in all structures since the polymeric chains with the strong covalent bonds are aligned better in that direction (see Fig. 2a). (d) Calculated X-ray diffraction patterns at 300 K for our pristine and interpenetrated COF-300 structures showing enhanced crystallinity quantified by the increased number of peaks in the diffraction pattern with interpenetration. Calculated thermal conductivities as a function of temperature for the pristine COF-300 and interpenetrated frameworks compared to thermal conductivities of the sum of 2 and 3 frameworks (signifying parallel channels of heat transfer without the influence of supramolecular interactions) in the (e) in-plane and (f) cross-plane directions. As is clear, supramolecular interactions in the interpenetrated frameworks result in considerably higher thermal conductivities as compared to the 2× and 3× thermal conductivities (especially at lower temperatures). This demonstrates the significant enhancement in thermal transport of the individual frameworks in the interpenetrated structures resulting from the supramolecular interactions.

Firstly, the thermal conductivity sum of 2 and 3 COF-300 frameworks is considerably lower than the corresponding 2IP and 3IP COF-300 systems at room temperature (and also at lower temperatures for both in-plane, Fig. 4e, and cross-plane directions, Fig. 4f). This difference is reduced at higher temperatures, and for the in-plane direction, we find that the sum of the parallel thermal transport channels of COF-300 frameworks are similar to that of the interpenetrated structure. This suggests that the supramolecular interactions facilitating heat transfer is especially prevalent at lower temperatures where there are reduced anharmonic effects. This is inline with our MSD calculations where we observe a larger difference at lower temperatures for the interpenetrated structures as compared to the single framework (Fig. 4b). Secondly, the effect of supramolecular interactions on thermal transport is larger in the cross-plane direction, which leads to the reduction in the anisotropy for our 3IP COF-300 as compared to the COF-300 framework (Fig. 3e). As mentioned above, the cross-plane direction has a relatively lower heat conduction efficiency due to the misoriented linkers along that direction (see Fig. 2a). Therefore, interpenetration can have a larger impact through the placement of parallel channels of heat flow as depicted by the arrows in Fig. 3b. This is also evident from the enhanced cross-plane thermal conductivity of the 3-fold interpenetrated COF-300 structure as compared to the $3 \times \kappa_{\text{COF-300}}$ across the entire temperature range (Fig. 4f). Taken together, depending on the direction along which we are considering the heat conduction (since the polymeric chain alignment can vary drastically in the different directions in COFs), interpenetration can have varying effects on the thermal transport mechanisms.

Sezginel *et al.*[30] have demonstrated that interpenetration of an idealized MOF with another guest MOF structure can lead to as much as ~2× increase in thermal conductivity. This is expected since additional channels of thermal transport are introduced through interpenetration, which can be predicted by a linear sum of the thermal conductivities of the two frameworks (considering the ideal scenario where framework–framework interactions do not lead to additional phonon scattering). As shown in Fig. 4e and f, this linear summation considerably underpredicts the thermal conductivity of our interpenetrated structures (especially at lower temperatures) since this simple model neglects the influence of supramolecular interactions. The idealized MOF structures studied by Sezginel *et al.*[30] are considerably different as compared to our interpenetrated COF-300 structures because the idealized systems are not able to replicate the interactions between the molecular functional groups that can significantly influence the vibrational landscape of interpenetrated organic-based

frameworks as shown for our COF-300 interpenetrated structures in Fig. 4a. These comparisons further highlight the influence of supramolecular interactions between the organic functional groups in enhancing thermal transport of interpenetrated polymeric frameworks.

Finally, we demonstrate the significant role played by supramolecular interactions on the thermal transport properties of interpenetrated COFs by modifying the interaction strengths between the individual frameworks *via* hydrostatic strain (as schematically illustrated in Fig. 5a). Not surprisingly, hydrostatic compressions lead to enhancements in thermal conductivity for the interpenetrated structures as shown in Fig. 5b and c for the in-plane and cross-plane directions, respectively. In contrast, no significant increase in thermal conductivity of the pristine COF-300 is observed under hydrostatic compression. This again shows that supramolecular interactions that are enhanced by bringing the individual frameworks closer together in our interpenetrated structures facilitate heat transfer, whereas the absence of these reinforcing interactions in the pristine COF-300 framework results in negligible influence on thermal transport with hydrostatic compression. It is also interesting to note that the application of hydrostatic tension increases the thermal conductivity of our pristine COF-300 structure in all directions, whereas it leads to a reduction in the thermal conductivity of the interpenetrated frameworks. This is a direct consequence of the reduced supramolecular interactions in the latter where the frameworks move farther apart from each other due to hydrostatic tension. This is reflected in the vibrational DOS (Fig. S8 and S9†) calculations where hydrostatic tension leads to softening of the phonons in the interpenetrated structures, whereas vibrational hardening is observed in the pristine COF-300 framework, thus resulting in the vastly different responses to the application of hydrostatic strain.

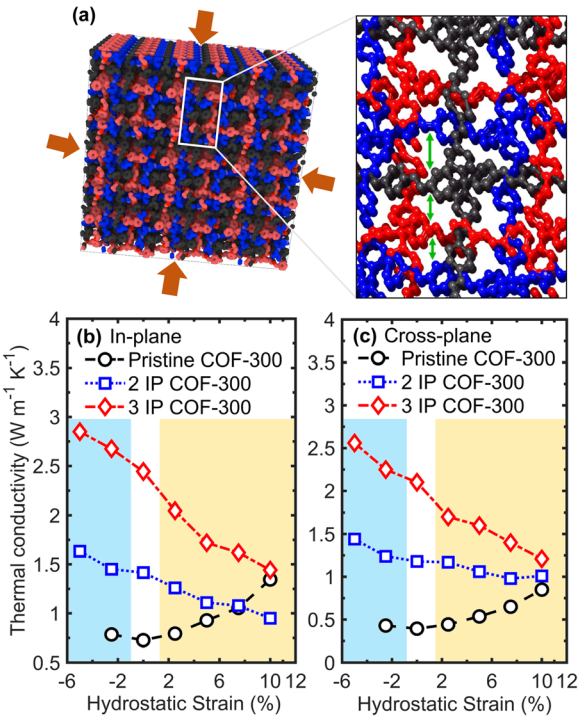

Fig. 5 (a) Schematic of our 3-fold interpenetrated COF-300 structure highlighting the supramolecular interactions between the individual COF-300 frameworks that can be modified *via* the application of varying levels of hydrostatic strain. Note, hydrogen atoms have been omitted for clarity. Room temperature thermal conductivities as a function of hydrostatic strain for our pristine, 2IP, and 3IP COF-300 structures in the (b) in-plane and (c) cross-plane directions. The blue and yellow shaded regions represent hydrostatic compression and tension, respectively. For both the 2IP and 3IP interpenetrated structures, thermal conductivities decrease monotonically as a function of hydrostatic tensile strain, whereas they increase with compression. With the application of hydrostatic tensile strains, the supramolecular interactions between the individual frameworks in the interpenetrated structures are reduced since the frameworks are pulled further apart from each other resulting in lower thermal conductivities in both the in-plane and cross-plane directions. In contrast, hydrostatic strain has significantly different effect on the single COF-300 framework (without the supramolecular interactions), where hydrostatic tension results in better alignment of the polymer chains (see Fig. S11†) and therefore results in higher thermal conductivities.

In summary, we have performed systematic atomistic simulations on COF-300 and its' interpenetrated structures to unravel the prominent role of supramolecular interactions in dictating the thermal transport mechansims in these polymeric framework materials. More specifically, we have shown that interpenetration of COF-300 results in significant enhancement (by upto 6-fold at room temperature) in their thermal conductivities as compared to the single COF-300 structure resulting from the reinforcing interactions between the individual frameworks. The supramolecular interactions between the COF-300 frameworks result in considerable phonon hardening and lattice stiffening thus explaining the enhancement in the thermal conductivities. We have also shown a drastically reduced anisotropy and a more crystalline-like behavior in the thermal conductivity trend with temperature for our interpenetrated structures. Furthermore, we have shown that these materials are mechanically flexible possessing modular elastic moduli (in the 1–13 GPa range) that can be achieved *via* varying degrees of interpenetration. Overall, our results highlight the significant role of interpenetration and supramolecular interactions in dictating the mechanical and thermal properties of 3D COFs, positioning them as lightweight and flexible materials with high thermal conductivities. This paves the way for strategic engineering of physical properties of polymeric frameworks *via* varying levels of interpenetration to fit the various needs in a variety of applications such as in flexible electronics, catalysis, and gas separation and storage to name a few.

Conflicts of interest

There are no conflicts to declare.

Acknowledgements

This work is supported by the Office of Naval Research, Grant no. N00014-21-1-2622. The work is also partially supported by the National Science Foundation (NSF Award no. 2119365).

References

1 A. M. Evans, A. Giri, V. K. Sangwan, S. Xun, M. Bartnof, C. G. Torres-Castanedo, H. B. Balch, M. S. Rahn, N. P. Bradshaw, E. Vitaku, et al., *Nat. Mater.*, 2021, **20**, 1142–1148.

2 K. Liu, B. Ouyang, X. Guo, Y. Guo and Y. Liu, *npj Flexible Electron.*, 2022, **6**, 1.

3 Z. Xie, B.-L. Hu, R.-W. Li and Q. Zhang, *ACS Omega*, 2021, **6**, 9319–9333.

4 H. Liu, H. Li, Z. Wang, X. Wei, H. Zhu, M. Sun, Y. Lin and L. Xu, *Adv. Mater.*, 2022, **34**, 2270348.

5 S. I. Rich, R. J. Wood and C. Majidi, *Nat. Electron.*, 2018, **1**, 102–112.

6 L. K. Reb, M. Böhmer, B. Predeschly, S. Grott, C. L. Weindl, G. I. Ivandekic, R. Guo, C. Dreißigacker, R. Gernhäuser, A. Meyer, et al., *Joule*, 2020, **4**, 1880–1892.

7 X. Li, P. Li, Z. Wu, D. Luo, H.-Y. Yu and Z.-H. Lu, *Mater. Rep.: Energy*, 2021, **1**, 100001.

8 P. She, Y. Qin, X. Wang and Q. Zhang, *Adv. Mater.*, 2022, **34**, 2101175.

9 Y. Shi, J. Yang, F. Gao and Q. Zhang, *ACS Nano*, 2023, **17**, 1879–1905.

10 H.-C. Zhou, J. R. Long and O. M. Yaghi, *Chem. Rev.*, 2012, **112**, 673–674.

11 O. M. Yaghi, M. J. Kalmutzki and C. S. Diercks, *Introduction to Reticular Chemistry: Metal-Organic Frameworks and Covalent Organic Frameworks*, John Wiley & Sons, 2019.

12 R. P. Bisbey and W. R. Dichtel, *ACS Cent. Sci.*, 2017, **3**, 533–543.

13 A. Giri, A. M. Evans, M. A. Rahman, A. J. McGaughey and P. E. Hopkins, *ACS Nano*, 2022, **16**, 2843–2851.

14 M. A. Rahman, C. J. Dionne and A. Giri, *Nano Lett.*, 2022, **22**, 8534–8540.

15 S. Thomas, H. Li, R. R. Dasari, A. M. Evans, I. Castano, T. G. Allen, O. G. Reid, G. Rumbles, W. R. Dichtel, N. C. Gianneschi, et al., *Mater. Horiz.*, 2019, **6**, 1868–1876.

16 A. M. Evans, M. J. Strauss, A. R. Corcos, Z. Hirani, W. Ji, L. S. Hamachi, X. Aguilar-Enriquez, A. D. Chavez, B. J. Smith and W. R. Dichtel, *Chem. Rev.*, 2021, **122**, 442–564.

17 F. Kang, X. Wang, C. Chen, C.-S. Lee, Y. Han and Q. Zhang, *J. Am. Chem. Soc.*, 2023, **145**, 15465–15472.

18 F. Jin, H. L. Nguyen, Z. Zhong, X. Han, C. Zhu, X. Pei, Y. Ma and O. M. Yaghi, *J. Am. Chem. Soc.*, 2022, **144**, 1539–1544.

19 G. Lin, H. Ding, D. Yuan, B. Wang and C. Wang, *J. Am. Chem. Soc.*, 2016, **138**, 3302–3305.

20 T. Ma, E. A. Kapustin, S. X. Yin, L. Liang, Z. Zhou, J. Niu, L.-H. Li, Y. Wang, J. Su, J. Li, et al., *Science*, 2018, **361**, 48–52.

21 Q. Zhu, X. Wang, R. Clowes, P. Cui, L. Chen, M. A. Little and A. I. Cooper, *J. Am. Chem. Soc.*, 2020, **142**, 16842–16848.

22 F. J. Uribe-Romo, J. R. Hunt, H. Furukawa, C. Klock, M. O'Keeffe and O. M. Yaghi, *J. Am. Chem. Soc.*, 2009, **131**, 4570–4571.

23 T. Ma, J. Li, J. Niu, L. Zhang, A. S. Etman, C. Lin, D. Shi, P. Chen, L.-H. Li, X. Du, et al., *J. Am. Chem. Soc.*, 2018, **140**, 6763–6766.

24 G. Chakraborty, I.-H. Park, R. Medishetty and J. J. Vittal, *Chem. Rev.*, 2021, **121**, 3751–3891.

25 H.-L. Jiang, T. A. Makal and H.-C. Zhou, *Coord. Chem. Rev.*, 2013, **257**, 2232–2249.

26 Y.-N. Gong, D.-C. Zhong and T.-B. Lu, *CrystEngComm*, 2016, **18**, 2596–2606.

27 M. Gupta and J. J. Vittal, *Coord. Chem. Rev.*, 2021, **435**, 213789.

28 J. Yang, T. Hu and T. C. Mak, *Cryst. Growth Des.*, 2014, **14**, 2990–3001.

29 L. Ma and W. Lin, *Angew. Chem.*, 2009, **121**, 3691–3694.

30 K. B. Sezginel, P. A. Asinger, H. Babaei and C. E. Wilmer, *Chem. Mater.*, 2018, **30**, 2281–2286.

31 C. J. Dionne, M. A. Rahman, P. E. Hopkins and A. Giri, *Nano Lett.*, 2022, **22**, 3071–3076.

32 J. Wieme, S. Vandenbrande, A. Lamaire, V. Kapil, L. Vanduyfhuys and V. Van Speybroeck, *ACS Appl. Mater. Interfaces*, 2019, **11**, 38697–38707.

33 H. Babaei, M. E. DeCoster, M. Jeong, Z. M. Hassan, T. Islamoglu, H. Baumgart, A. J. McGaughey, E. Redel, O. K. Farha, P. E. Hopkins, et al., *Nat. Commun.*, 2020, **11**, 4010.

34 M. Islamov, H. Babaei, R. Anderson, K. B. Sezginel, J. R. Long, A. J. McGaughey, D. A. Gomez-Gualdron and C. E. Wilmer, *npj Comput. Mater.*, 2023, **9**, 11.

35 B. Huang, A. McGaughey and M. Kaviany, *Int. J. Heat Mass Transfer*, 2007, **50**, 393–404.

36 X. Zhang and J. Jiang, *J. Phys. Chem. C*, 2013, **117**, 18441–18447.

37 H. Babaei, A. J. McGaughey and C. E. Wilmer, *Chem. Sci.*, 2017, **8**, 583–589.

38 H. Babaei and C. E. Wilmer, *Phys. Rev. Lett.*, 2016, **116**, 025902.

39 L. Han, M. Budge and P. A. Greaney, *Comput. Mater. Sci.*, 2014, **94**, 292–297.

40 H. Babaei, A. J. McGaughey and C. E. Wilmer, *ACS Appl. Mater. Interfaces*, 2018, **10**, 2400–2406.

41 M. E. DeCoster, H. Babaei, S. S. Jung, Z. M. Hassan, J. T. Gaskins, A. Giri, E. M. Tiernan, J. A. Tomko, H. Baumgart, P. M. Norris, et al., *J. Am. Chem. Soc.*, 2022, **144**, 3603–3613.

42 K. J. Erickson, F. Léonard, V. Stavila, M. E. Foster, C. D. Spataru, R. E. Jones, B. M. Foley, P. E. Hopkins, M. D. Allendorf and A. A. Talin, *Adv. Mater.*, 2015, **27**, 3453–3459.

43 A. Lamaire, J. Wieme, A. E. Hoffman and V. Van Speybroeck, *Faraday Discuss.*, 2021, **225**, 301–323.

44 S. Zhang, J. Liu and L. Liu, *RSC Adv.*, 2021, **11**, 36928–36933.

45 R. Cheng, W. Li, W. Wei, J. Huang and S. Li, *ACS Appl. Mater. Interfaces*, 2021, **13**, 14141–14149.

46 P. Ying, J. Zhang and Z. Zhong, *J. Phys. Chem. C*, 2021, **125**, 12991–13001.

47 J. Huang, X. Xia, X. Hu, S. Li and K. Liu, *Int. J. Heat Mass Transfer*, 2019, **138**, 11–16.

48 M. Islamov, P. Boone, H. Babaei, A. J. McGaughey and C. E. Wilmer, *Chem. Sci.*, 2023, **14**, 6592–6600.

49 A. Giri and P. E. Hopkins, *Nano Lett.*, 2021, **21**, 6188–6193.

50 M. A. Rahman, C. J. Dionne and A. Giri, *ACS Appl. Mater. Interfaces*, 2022, **14**, 21687–21695.
51 H. M. Aktulga, J. C. Fogarty, S. A. Pandit and A. Y. Grama, *Parallel Comput.*, 2012, **38**, 245–259.
52 S. Plimpton, *J. Comput. Phys.*, 1995, **117**, 1–19.
53 C. Kittel and D. F. Holcomb, *Am. J. Phys.*, 1967, **35**, 547–548.
54 P. Klemens, *Proc. Phys. Soc. A*, 1955, **68**, 1113.
55 K. D. Parrish, A. Jain, J. M. Larkin, W. A. Saidi and A. J. McGaughey, *Phys. Rev. B*, 2014, **90**, 235201.